HHS Public Access

Author manuscript

Neuron. Author manuscript; available in PMC 2019 November 21.

Published in final edited form as:

Neuron. 2018 November 21; 100(4): 926–939.e3. doi:10.1016/j.neuron.2018.09.029.

Somatostatin Interneurons Facilitate Hippocampal-Prefrontal Synchrony and Prefrontal Spatial Encoding*

Atheir I. Abbas[1,2,**], **Marina J. M. Sundiang**[1,2], **Britt Henoch**[1,2], **Mitchell P. Morton**[1,2], **Scott S. Bolkan**[1,2], **Alan J. Park**[1,2], **Alexander Z. Harris**[1,2], **Christoph Kellendonk**[1,3], and **Joshua A. Gordon**[4,*]

[1]Department of Psychiatry, Columbia University, New York, New York 10032

[2]Division of Integrative Neuroscience, New York State Psychiatric Institute, New York, New York 10032

[3]Division of Molecular Therapeutics, New York State Psychiatric Institute, New York, New York 10032

[4]National Institute of Mental Health, Bethesda, MD 20892

Summary

Decreased hippocampal-prefrontal synchrony may mediate cognitive deficits in schizophrenia but it remains unclear which cells orchestrate this long-range synchrony. Parvalbumin- (PV) and somatostatin-expressing (SOM) interneurons show histological abnormalities in individuals with schizophrenia, and they are hypothesized to regulate oscillatory synchrony within the prefrontal cortex. To examine the relationship between interneuron function, long-range hippocampal-prefrontal synchrony, and cognition, we optogenetically inhibited SOM and PV neurons in the medial prefrontal cortex (mPFC) of mice performing a spatial working memory task while simultaneously recording neural activity in the mPFC and the hippocampus (HPC). We found that inhibiting SOM, but not PV, interneurons during the encoding phase of the task impaired working memory accuracy. This behavioral impairment was associated with decreased hippocampalprefrontal synchrony and impaired spatial encoding in mPFC neurons. These findings suggest that interneuron dysfunction may contribute to cognitive deficits associated with schizophrenia by disrupting long range synchrony between the HPC and PFC.

*The opinions expressed in this article are the authors' own and do not reflect the view of the National Institutes of Health, the Department of Health and Human Services or the United States government.

*Additional Corresponding Author: J.A.G. (joshua.gordon@nih.gov).

**Lead Contact:
A.I.A. (aia2114@cumc.columbia.edu

Author Contributions

A.I.A. and J.A.G. designed the experiments. A.I.A. performed experiments and analyzed the data. M.J.M.S., B.H., and M.P.M. assisted in performing experiments. S.S.B., A.J.P., A.Z.B., C.K., and J.A.G. assisted in analysis of experiments. A.I.A., A.Z.B., C.K., and J.A.G. interpreted the results and wrote the article.

Declaration of Interests

The authors declare no competing interests.

eTOC Blurb

Abbas et al. examine the role of somatostatin and parvalbumin interneurons during spatial working memory. They found that, somatostatin, but not parvalbumin interneurons, support working memory performance by facilitating hippocampalprefrontal interactions and associated spatial encoding.

Keywords

Somatostatin; parvalbumin; interneuron; working memory; hippocampal-prefrontal; prefrontal cortex; synchrony; theta; inhibitory neuron; encoding; oscillations

Introduction

Working memory, a critical cognitive function, is impaired in schizophrenia (Park and Holzman, 1992; Saykin et al., 1991; Saykin et al., 1994) and other psychiatric disorders (Arts et al., 2008; Lai et al., 2016; Landro et al., 2001; Martinussen R, 2005). Cognitive impairments contribute significantly to poor functioning (Brekke et al., 2007; Green, 2016; Green et al., 2000; Keefe et al., 1999), and available treatments do not effectively treat these impairments. Thus, elucidating the neural basis for cognitive symptoms in psychiatric disorders may inform new treatment strategies that reduce the functional impact of disease.

In rodents, working memory for spatial information is thought to be supported by interactions between multiple brain regions. Three lines of evidence implicate the mPFC and HPC. First, oscillatory synchrony between these structures, particularly in the theta (4–12 Hz) and gamma (40–80) Hz range, is enhanced during spatial working memory tasks (Hallock et al., 2016; Jones and Wilson, 2005; Lagler et al., 2016; O'Neill et al., 2013; Sigurdsson et al., 2010). Second, pharmacological inhibition of neural activity in HPC or mPFC, lesioning of these regions, and anatomical disconnection of mPFC and HPC impairs working memory performance (Churchwell and Kesner, 2011; Lee and Kesner, 2003; Urban et al., 2014; Wang and Cai, 2006). Third, selective optogenetic inhibition of the projection from the ventral HPC (vHPC) to the mPFC during spatial working memory encoding impairs the representation of spatial information in mPFC neurons and decreases task performance accuracy (Spellman et al., 2015).

These data demonstrate the significance of HPC-mPFC circuit activity, and in particular, the direct projection from the HPC to the mPFC, in the encoding of spatial representations critical for working memory. However, the cellular subtypes within the mPFC that mediate these interactions between HPC and mPFC are poorly characterized. Given that these interactions involve oscillatory activity, and that interneurons are hypothesized to play a key role in driving oscillatory synchrony, we hypothesized that interneurons, which receive hippocampal excitatory inputs (Parent et al., 2010), may be crucial for maintaining these long-range interactions.

Two types of interneurons, PV and SOM interneurons, have attracted attention because both mRNAs are decreased in the PFC of individuals with schizophrenia (Fung et al., 2014; Fung

et al., 2010; Hashimoto et al., 2008; Hashimoto et al., 2003). PV interneurons target soma and perisomatic compartments of pyramidal cells thereby controlling their spiking output (Atallah et al., 2012; Kvitsiani et al., 2013). In contrast, SOM interneurons target distal dendrites, which is important for gating pyramidal cell inputs (Gentet et al., 2012; Kvitsiani et al., 2013; Silberberg and Markram, 2007). We therefore hypothesized SOM interneurons are well positioned to regulate coordination with long range inputs, whereas PV interneurons may support working memory by organizing local activity within the PFC.

To test this hypothesis, we optogenetically inhibited prefrontal PV or SOM interneurons in the mPFC of mice performing a spatial working memory task. We simultaneously recorded neural activity in the mPFC and other brain areas known to be involved in working memory, including the dorsal and ventral hippocampus (dHPC and vHPC), and mediodorsal thalamus (MD) (Parnaudeau et al., 2013). We found that inhibiting SOM but not PV interneurons impaired working memory when inhibition was performed during the encoding phase. Furthermore, by examining the above-described working memory circuit, we found that the working memory impairment that resulted from SOM inhibition was associated with decreased long range synchrony between HPC and mPFC, decreased HPC to mPFC directionality of that long range coordination, and impaired mPFC spatial encoding. We conclude that SOM interneurons facilitate hippocampal-prefrontal synchrony and support mPFC spatial encoding necessary for working memory.

Results

Somatostatin interneurons are required for spatial working memory

To examine the role of mPFC interneurons in spatial working memory, we inhibited PV and SOM interneurons during different phases of a delayed non-match to sample T-maze task (Bolkan et al., 2017; O'Neill et al., 2013; Sigurdsson et al., 2010). Each trial consists of three phases, a forced sample run in which the animal encodes the environment, a delay phase in which the animal has to maintain information, and a choice phase in which the mouse must retrieve the previously encoded and maintained information to make a correct choice – the arm not visited during the sample phase (Figure 1A and methods). To selectively target PV and SOM interneurons we injected Cre-inducible eArch3.0-YFP adeno-associated-virus (AAV5-EF1a-DIO-eArch3.0-EYFP) (Chow et al., 2010; Mattis et al., 2011) in SOM-Cre (Taniguchi et al., 2011) or PV-Cre (Lovett-Barron et al., 2012) mice, which leads to selective expression of eArch3.0-YFP in SOM (SOM-Arch, Figure S1A and S1C-1D) or PV (PV-Arch, Figure S1B and S1E-1F) interneurons. We also injected a subset of SOM-Cre and PV-Cre animals with Creinducible YFP adeno-associated-virus to control for nonspecific effects. Mice were implanted with custom optoelectrodes to permit simultaneous illumination and neural recordings within the mPFC. They were also implanted with single wire electrodes to facilitate recordings of local field potentials (LFPs) in the vHPC, dHPC, and MD.

Upon illumination of the mPFC in both SOM-Cre and PV-Cre mice, a subset of neurons exhibited a significant decrease in firing rate (Figure 1B-1C, 2A, 2C, and S2A-S2D). Firing rates increased in a larger subset of neurons (Figure 1B, 1D, 2B-2C, and S2A-S2D). The percentage of cells with increased and decreased firing rates in response to light in mPFC

varied only slightly as a function of the phase of the task during which the light was delivered, and a much higher percentage of neurons was light-modulated in Arch-expressing mice compared to YFP-expressing mice (Figure 1B, 2C, and S2A-S2D). Light modulated neurons also had a larger change in firing rate in response to green light in Arch mice as compared to control YFP mice (Figure S1G-1H; Firing rate expressed as % of baseline, SOM-Arch vs SOM-YFP, Increasers: Sample – 265.2%+/−14.7% vs 127.7%+/−4.7%; Delay – 256.6%+/−13.3% vs 126.2%+/−2.4%; Choice 320.9%+/−29.4% vs 151.6%+/−4.5%; SOM-Arch vs SOM-YFP, Decreasers: Sample – 61.4%+/−2.5% vs 82.9%+/−1.2%; Delay – 62.2%+/−2.5% vs 82.8%+/−1.2%; Choice – 62.0%+/−2.7% vs 72.6%+/−1.9%; PV-Arch vs PV-YFP, Increasers: Sample – 415.7%+/−104.9% vs 144.9%+/−8.1%; Delay – 266.8%+/−24.6% vs 158.0%+/−18.9%; Choice – 352.2%+/−78.1% vs 185.3%+/−15.8%; PV-Arch vs PV-YFP, Decreasers: Sample – 66.1%+/−3.2% vs 77.6%+/−2.3%; Delay – 69.4%+/−3.1% vs 76.6%+/−2.5%; Choice – 65.5%+/−2.3% vs 60.6%+/−3.5%). These findings are consistent with lightinduced inhibition of PV- or SOM-expressing interneurons, leading to disinhibition of pyramidal neurons. Attempts to confirm cell identity by examining waveform shape (Courtin et al., 2014; Kim et al., 2016) were not successful (see Methods for details and Figure S1I-1J). We will therefore refer to these groups of neurons as putative SOM, PV, or pyramidal neurons, or more simply, “increasers” and “decreasers,” throughout the rest of the article.

Behavioral performance was measured in the same mice. During randomly interleaved trial types, SOM or PV interneurons were either not inhibited or inhibited during the sample, delay, or choice phases of the DNMTS task. The delay phase length was varied on different days of testing to either 10 or 60 seconds. We found that inhibiting SOM interneurons during the sample phase, but not the delay or choice phases, led to a significant decrease in spatial working memory performance when the delay was 60 seconds (Figure 3B-3C, SOM-Arch, N = 17 mice; SOM-YFP, N = 15 mice; 2-way repeated measures ANOVA, significant virus x light interaction, $F(3,90) = 3.199$, $p = 0.0271$; and OFF vs Sample On significant by post-hoc testing Bonferroni corrected for multiple comparisons, $p=0.0001$), but not 10 seconds (Figure 3A, SOM-Arch, N = 14 mice; SOM-YFP, N = 14 mice; 2-way repeated measures ANOVA, no significant virus x light interaction, $F(3,78) = 0.5113$, $p = 0.6757$). In contrast, we found that inhibiting PV interneurons in PV-Arch animals during any of the phases, sample, delay, or choice, had no effect on working memory performance at 10 second delay (Figure 3D, PV-Arch, N = 10 mice; PV-YFP, N = 7 mice; 2-way repeated measures ANOVA, no significant virus x light interaction, $F(3,45) = 0.7777$, $p = 0.5126$) or 60 second delay (Figure 3E-3F, PV-Arch, N = 10 mice; PV-YFP, N = 7 mice; 2-way repeated measures ANOVA, no significant virus x light interaction, $F(3,45) = 0. 4708$, $p = 0. 7041$).

Somatostatin interneurons facilitate long range synchrony

SOM interneurons target distal dendrites, gating pyramidal cell inputs (Gentet et al., 2012; Kvitsiani et al., 2013; Silberberg and Markram, 2007). PV interneurons target soma and perisomatic compartments of pyramidal cells thereby controlling their spiking output (Atallah et al., 2012; Kvitsiani et al., 2013). We therefore hypothesized that SOM inhibition might decrease hippocampal-prefrontal synchrony while PV inhibition might modulate local mPFC oscillatory activity. We restricted our analysis to data from the 60 second delay

experiments since this was where we saw a significant behavioral effect in SOM mice. Before examining oscillatory synchrony, we began by characterizing the effect of optogenetic manipulation of SOMs and PVs on oscillatory power within the mPFC. We found that inhibiting SOMs and PVs by delivering green light in the mPFC during the sample phase led to a significant increase in broadband power locally in the mPFC, while delivering green light in SOM-YFP and PV-YFP animals did not affect mPFC power (Figure 4A-4D). More generally, inhibiting SOMs during all three phases led to a significant increase in power across a broad range of frequencies (Figure S3A), including an increase in power in the dHPC and MD (Figure S3C). In contrast, while inhibiting PVs during the sample, delay, or choice phase led to an increase in beta (12–25 Hz) and gamma (30–70 Hz) power, only delay (and not sample or choice) phase inhibition increased mPFC theta power (Figure S3B), while power in other regions was unaffected (Figure S3D). Neither SOM nor PV inhibition affected behavioral covariates of theta power including running speed or trial length during the different phases (Figure S3E-S3F). Overall, these findings support a role for both SOMs and PVs in shaping local mPFC oscillatory activity.

We next examined whether SOMs supported hippocampal-prefrontal synchrony as we hypothesized. To do this, we compared long-range synchrony in SOM-Arch and PV-Arch mice. We found that coherence between oscillatory activity in the LFPs in the mPFC and LFPs in the vHPC, dHPC, or MD was globally decreased with SOM inhibition regardless of task phase, while the decrease in coherence was less consistent and smaller in magnitude with PV inhibition (Figure 4E-4F and Figure S4). To ensure that these changes in oscillatory synchrony reflect local cellular activity rather than volume conduction, we examined the phase-locking of single units in the mPFC to oscillations in the HPC using a measure of phase locking called pairwise phase consistency (PPC), focusing on theta-frequency oscillations since phase-locking to theta oscillations has been linked to spatial working memory (Hallock et al., 2016; Jones and Wilson, 2005; Lagler et al., 2016; O'Neill et al., 2013; Sigurdsson et al., 2010). Phase locking of mPFC single units to vHPC and dHPC theta decreased during SOM sample phase inhibition (Figure 5A-5D). This decrease in phase locking was frequency and pathway specific as SOM inhibition did not decrease phase-locking to MD theta or to other frequencies in vHPC, dHPC, or MD with the exception of a decrease in phase locking of "decreasers" to MD gamma (Figure S5A-5C). We also found that SOM inhibition increased phase locking of "increasers" to dHPC and MD beta oscillations and MD gamma oscillations. The effects of SOM inhibition on theta synchrony were specific for putative pyramidal neurons – we found that "increasers" decreased phase-locking to vHPC and dHPC theta after SOM inhibition, whereas the phase-locking of "decreasers" was unchanged (Figure 5C-D, middle and right column). Notably, SOM inhibition significantly increased phase locking to local mPFC theta, beta, and gamma oscillations (Figure 5E–5F and S5D), suggesting that reduced long-range input increases the degree to which mPFC neurons are driven by local activity. In contrast to SOM inhibition, we found that PV inhibition did not affect mean phase-locking to vHPC, dHPC, or MD theta oscillations either for all units, or for "increasers" or "decreasers" (Figure S6A-6C), though PV inhibition leads to an even larger increase in phase locking to local mPFC theta, beta, and gamma oscillations as compared to the significant increase seen with SOM inhibition (Figure 5G-5H and S5E). Overall, these findings suggest that inhibiting SOM interneurons

has a stronger impact on hippocampalprefrontal synchrony than does inhibiting PV interneurons, whereas inhibiting both SOMs and PVs has a robust effect on local mPFC activity, with PV inhibition affecting local synchrony more than SOMs.

Somatostatin interneurons disrupt the directionality of ventral hippocampalprefrontal synchrony

To corroborate the findings of reduced hippocampal-prefrontal synchrony, we examined the directionality of hippocampal-prefrontal theta-frequency interactions during SOM inhibition. In order to assess directionality, we performed a lag analysis, calculating phase-locking of mPFC neurons to vHPC and dHPC theta oscillations at a range of lags. During light OFF trials, phase-locking to both vHPC and dHPC theta was stronger at negative lags compared to positive lags, suggesting a predominantly HPCto-mPFC directionality (Figure 6A-6B and 6D-6E). However, with sample phase SOM inhibition, phase-locking to vHPC theta at negative lags was no longer significantly different from that at positive lags (figure 6C), suggesting that SOM inhibition disrupted the net directionality between vHPC and mPFC, consistent with a disruption in vHPC-tomPFC communication. Interestingly, sample phase SOM inhibition did not affect dHPCmPFC directionality (Figure 6F), consistent with previous findings demonstrating that inhibition of vHPC terminals in the mPFC did not disrupt phase-locking to dHPC theta (Spellman et al., 2015). Overall, these findings further support a role for SOMs in facilitating information flow from the HPC to the mPFC.

Somatostatin interneurons are necessary for spatial encoding in the mPFC

Decreased hippocampal-prefrontal synchrony indicates impaired long range communication between these structures; such communication is critical for the representation of spatial information in the mPFC (Spellman et al., 2015). Indeed, a subpopulation of mPFC neurons encode the goal arm location visited by the mouse during the sample phase, and inhibition of vHPC inputs to the mPFC disrupts this goal arm encoding and later choice performance (Bolkan et al., 2017; Spellman et al., 2015). As SOM interneuron inhibition similarly impairs vHPC-mPFC synchrony and choice performance, we examined whether SOM inhibition affects goal arm encoding. During laser off trials, many mPFC neurons tended to fire more actively at one of the two goal arms (Figure 7A). This arm preference was abolished by SOM inhibition (Figure 7A). In contrast, goal arm preference was preserved with PV inhibition (Figure 7B). To understand why SOM and PV inhibition had differing effects on goal arm preferences, we compared the effects of inhibition on firing rates in spatially tuned neurons and nonspatially tuned neurons. SOM inhibition led to a more robust increase in firing rates across tuned (both preferred and non-preferred arm firing) and non-tuned neurons in comparison to PV inhibition around the time of sample goal arrival (Figure 7C-7E). We also examined whether putative SOM and PV neurons themselves entrain differently to vHPC and dHPC theta, but no difference in entrainment was observed (Figure 7F-7G). These data demonstrate that though both SOM and PV interneurons participate in HPCentrained rhythmic activity in the theta-range, SOM interneuron inhibition has a greater effect on mPFC neuronal firing rates and neuronal goal arm preferences during working memory encoding.

To confirm the effects of SOM inhibition on spatial encoding, we used a maximum margin linear classifier to decode mouse location from vectors of binned firing rates of recorded mPFC units (Rigotti et al., 2013; Spellman et al., 2015). The decoder was trained to extract mouse location using a subset of the trials in which the laser was off during the sample phase. Decoder accuracy was tested on another subset of the laser off trials and compared to accuracy when testing in trials in which the laser was on during the sample phase (as in Spellman, 2015). In SOM-Arch animals, decoder accuracy was degraded when tested in laser on sample trials as compared to laser off trials (Figure 7H). No such degradation was seen in SOM-YFP or PV-Arch mice (Figure 7I-7J; two-way repeated measures ANOVA comparing decoder performance between off and sample on trials across SOM-Arch, SOM-YFP, and PV-Arch mice, significant effect of virus, $F(2, 78) = 44.49$, and laser condition, $F(1, 78) = 48.17$, with significant virus x laser condition interaction, $F(2, 78) = 20.64$, $p<0.0001$ for all three; there was a significant decrease in decoder accuracy by Bonferroni-corrected post-hoc testing in SOM-Arch, but not SOM-YFP or PV-Arch mice, $p<0.0001$).

We also examined prospective sample goal coding, which has previously been reported (Guise and Shapiro, 2017), during the sample phase (at the time the mouse is entering the intersection and is able to discern which goal will be the sample goal), and we found that it was impaired during laser on sample trials as compared to off trials or trials in which the laser will subsequently be on during the choice phase (Figure S7A, see below for statistical summary). In contrast, we found that prospective chosen goal coding during the choice phase was not affected by preceding sample phase or concurrent choice phase laser illumination (Figure S7B, two-way repeated measures ANOVA comparing decoder performance between off, sample on, and choice on trials across the sample and choice phases, significant effect of laser condition, $F(2, 40) = 7.783$, $p=0.0014$, and task phase, $F(1, 20) = 5.93$, $P=0.0244$, with significant virus x task phase interaction, $F(2, 40) = 33.39$, $p<0.0001$; there was a significant decrease in decoder accuracy by Bonferroni-corrected post-hoc testing with sample phase inhibition, $p<0.0001$, but not in other laser conditions or during the choice phase). These findings support a role for somatostatin interneurons in supporting representations of spatial information specifically during sample phase encoding.

Somatostatin interneuron activity during working memory encoding is necessary for subsequent delay period activity

We have previously reported that during working memory maintenance, groups of neurons transiently increase their firing rate sequentially across the delay phase, and this activity is necessary for normal working memory performance (Bolkan et al., 2017). Because SOM inhibition impairs the formation of spatial representations during working memory encoding, we hypothesized that impaired working memory encoding would disrupt subsequent sequential delay phase activity. We found that SOM inhibition during the sample phase did indeed disrupt sequential activity during the subsequent delay phase (Figure 8A). SOM inhibition during the delay phase itself appears to lead to a robust increase in overall firing in a subset of cells across the delay period (consistent with Figures 1–2 and S1-S2), making it difficult to visualize transiently elevated cells. Sequential activity during the delay not surprisingly appeared unaffected during choice trials, in which the SOM inhibition occurred after the delay.

We compared the distributions of times at which the peak firing rate occurred in delay-elevated cells across the population of recorded neurons in the different conditions – OFF, On Sample, On Delay, and On Choice – using the Kolmogorov-Smirnov test. This revealed that the tiling was altered in the On Sample condition only – (OFF vs On Samp, P value = 0.0002; OFF vs On Del, P value = 0.1192; OFF vs On Choice, P value = 0.8752). Thus, SOM inhibition during the sample phase disrupts subsequent delay tiling, whereas concurrent SOM inhibition during the delay does not, despite dramatically altering firing rates. Since we have previously reported that disruptions of delay-elevated firing also decreased the firing rate at peak, we grouped cells by the timing of their firing rate peaks and calculated the mean firing rate over the period of the delay around the peak. One-way ANOVA followed by Bonferronicorrected pairwise comparisons over the whole delay (excluding directly manipulated on delay trials for the analysis) indicated that there was a significant effect of laser condition on the firing rate of delay-elevated cells ($F(2,702) = 8.271$, P-value = 0.0003; off vs on sample post-hoc p-value < 0.0002). When we grouped cells by the timing of their peak firing and calculated mean firing rate over the period around that time, we found that sample phase SOM inhibition (On Samp) preceding the delay phase significantly decreased normalized firing rates in delay-elevated neurons after the first 10 seconds of the delay phase (Figure 8B; one-way ANOVA to examine the effect of laser condition; 1–10 s – $F(2,309) = 1.115$, P-value = .3293; 11–20 s – $F(2,102) = 8.533$, P-value = 0.0004; 21–40 s – $F(2,177) = 19.23$, P-value < 0.0001; 41–60 s – $F(2,105) = 5.189$, P-value = 0.0071).

In contrast, when we performed the same analysis in our PV-Arch animals, PV inhibition during the preceding sample phase did not affect subsequent delay period activity, whereas PV inhibition had a similar effect to SOM inhibition during the delay itself, increasing the baseline firing rate in a large subset of delay-elevated cells. Unlike SOM inhibition, with PV inhibition there was no significant effect of laser condition on the firing rate of delay-elevated cells (by one-way ANOVA, $F (2, 183) = 0.109$, P-value = 0.8968). PV inhibition did not disrupt the timing of delay period tiling (Figure S8A; not significant by Kolmogorov-Smirnov test; OFF vs On Samp, P value = 0. 3081; OFF vs On Del, P value = 0.0914; OFF vs On Choice, P value = 0.9207) or mean firing rate at peak (Figure S8B; one-way ANOVA to examine the effect of laser condition, 1–10 s – $F (3, 68) = 0.06114$, P-value = .9800; 11–20 s – $F (3, 24) = 0.422$, P-value = 0.7389; 21–40 s – $F (3, 76) = 0.08662$, P-value < 0.9672; 41–60 s – $F (3, 64) = 0.1419$, P-value = 0.9345). Together, these findings suggest that, unlike PV inhibition, SOM inhibition during the sample phase not only impairs hippocampal-prefrontal synchrony and spatial encoding during the sample phase, but also disrupts sequential firing patterns during the subsequent delay period.

Discussion

In this study we show differential roles of SOM and PV interneurons with respect to spatial working memory performance, long range synchrony, and spatial representations in the mPFC. We found that SOM, but not PV, interneurons were required during the sample phase of a spatial working memory task, suggesting a requirement for this neuronal subtype in encoding spatial information. Inhibition of either interneuron subtype during the delay (maintenance) or choice (retrieval) phases of the spatial working memory task had no effect

on memory performance. Furthermore, we found that while both SOM and PV inhibition led to a global enhancement in local mPFC power and phase locking to local oscillations, only SOM inhibition impaired hippocampal-prefrontal synchrony and associated hippocampal-to-prefrontal directionality, encoding of prefrontal spatial representations, and sequential activity of mPFC neurons during the subsequent delay period of the spatial working memory task. Our results demonstrate the importance of SOM, but not PV, interneurons in spatial working memory, suggesting that they subserve working memory encoding by facilitating information flow from the HPC to the mPFC.

Somatostatin interneurons during working memory

Our results show a previously unreported role for SOM interneurons during working memory. While previous studies have focused on a role for mPFC SOM interneurons during working memory maintenance, we found that mPFC SOM interneurons appear to be required only during spatial working memory encoding in the DNMTS T-maze task. A previous study reported that SOM interneurons encode spatial location during the delay phase of a similar spatial working memory task, and that activating these neurons during the delay impaired performance (Kim et al., 2016). We suspect that the discrepancy in behavioral findings is because optogenetic activation of SOM interneurons induces artificial patterns of activity which may confer a disruptive potential that does not reflect the normal role of SOM interneurons during working memory. Alternatively, task-specific differences may underlie the differing effects. Consistent with our previous results (Bolkan et al., 2017; Spellman et al., 2015), we found no evidence of retrospective coding of sample goal location during the delay period in our task, unlike in Kim et al. (Figure S6D-6F).

Task and brain region differences may explain differences between our data and those in a recent report examining the role of SOM interneurons in anterior cingulate cortex in a non-spatial Go/No-Go task (Kamigaki and Dan, 2017). In this study, optogenetic inhibition of SOM neurons during the whole trial or the delay phase improved performance, while optogenetic excitation impaired performance. Recent studies have suggested that the mPFC supports maintenance via MD input-dependent sequentially and transiently activated neuronal ensembles that are linked to attention or rule encoding rather than spatial encoding (Akhlaghpour et al., 2016; Bolkan et al., 2017; Fujisawa et al., 2008; Horst and Laubach, 2012; Rajan et al., 2016; Schmitt et al., 2017). It may be that such rule-encoding is susceptible to artificial SOM excitation (as in Kim et al., 2016) or inhibition during non-spatial tasks (as in Kamigaki et al., 2017). We found that delay phase SOM inhibition increases the overall delay firing rate such that it is difficult to resolve transient delay-elevated firing as previously reported. Despite this we find no effect of delay phase SOM inhibition on performance, suggesting the possibility that delay SOM inhibition increases background activity during the delay without disrupting information content or maintenance of memory traces. In contrast, we find that SOM inhibition preceding the delay during encoding disrupts delay-elevated firing, suggesting that without normal sample phase spatial encoding there is decreased progression to normal working memory maintenance-associated activity.

Parvalbumin interneurons during working memory

Our findings suggest that PV interneurons do not appear to be required for working memory, HPC-mPFC phase locking, spatial encoding, or delay-elevated firing. The failure of PV inhibition to influence these parameters is not due to an inadequate degree of PV manipulation as evidenced by robust effects of PV inhibition on mPFC firing rates, LFP power, and phase locking to local oscillations. The PV interneuron data are somewhat surprising given previous findings that PVs exhibit a range of taskrelated activity patterns and synchronize with HPC theta oscillations (Lagler et al., 2016). Previous studies have attempted to address the role of PV interneurons in working memory by manipulating mPFC PV interneuron function in various ways, though not using optogenetic inhibition. Results from these studies are inconsistent, with some suggesting a potential role for PV neurons in working memory (Gandal et al., 2012; Murray et al., 2015) and others arguing against such a role (Canetta et al., 2016; Carlen et al., 2012). Consistent with our findings, optogenetic activation of mPFC PV interneurons during the delay phase also did not significantly affect performance in a Figure-8 spatial working memory task (Kim et al., 2016). In contrast, during the above mentioned Go/No-Go task, where PV interneurons exhibit choice-biased activity, optogenetically stimulating PV interneurons in the nearby anterior cingulate cortex (ACC) during the delay period severely impaired task performance, whereas inhibiting them improved performance (Kamigaki and Dan, 2017).

As discussed above, this may be because different working memory tasks were used or because interneurons were recorded in ACC in the Go/No-Go task rather than PL/IL. It may also be a matter of sensitivity, in that although the effects of PV inhibition and SOM inhibition on mPFC firing rates are comparable, relatively more PV inhibition may be required to affect working memory. Furthermore, since SOMs and PVs arborize differently, it is also possible that the similar impact we see in terms of the proportion of neurons modulated by light and other parameters may nonetheless be associated with a lesser effect of PVs on local mPFC network activity in comparison to SOMs. We found that, although SOM and PV inhibition affect local mPFC power similarly and PV inhibition has a greater effect on phase locking to local mPFC oscillations in comparison to SOMs, PV inhibition has a lesser impact on the firing of mPFC neurons as compared to SOM inhibition around the time of sample goal arrival. Finally, PV interneurons are a heterogenous population and we may be suppressing two different subpopulations of PV interneurons, basket cells and chandelier cells, which could have opposing effects. Further work in targeting specific subpopulations of PV interneurons, or specific inputs to PV cells, and examining their role in different behaviors in different prefrontal regions should help illuminate their role in cognition more clearly.

Key cellular elements and connectivity in working memory

We provide here strong evidence for a requirement of SOM interneurons for spatial working memory. When SOM interneuron firing is suppressed during the sample period of a spatial working memory task, hippocampal-prefrontal synchrony and associated hippocampal to prefrontal directionality, prefrontal spatial encoding, and subsequent delay-elevated neuronal firing are impaired, resulting in decreased working memory performance. These findings build on previous studies showing that vHPCmPFC and dHPC-mPFC theta band synchrony

support spatial working memory (Jones and Wilson, 2005; O'Neill et al., 2013), and vHPC inputs to the mPFC are required for spatial encoding during the sample period of a spatial working memory task (Spellman et al., 2015). Thus, the findings we present here suggest that SOM interneurons are one of the specific cellular elements of the HPC-mPFC circuit that are required for information flow from the hippocampus to the prefrontal cortex.

As SOM interneurons gate apical dendrites of pyramidal neurons (Silberberg and Markram, 2007; Urban-Ciecko and Barth, 2016; Yavorska and Wehr, 2016), they are well positioned to coordinate long range synchrony between the HPC and the mPFC, thereby regulating HPC-mPFC information flow. SOM interneurons in some cortical areas receive direct long range inputs (Wall et al., 2016), suggesting the possibility that feedforward inhibition from the HPC to SOM interneurons in mPFC may mediate long synchrony between the two regions. In fact, recent work has shown that SOMs facilitate long range coherence within visual cortex (Veit et al., Nat Neurosci, 2017) and are important for synchronizing low frequency activity (Chen et al., Neuron, 2017), supporting a role for SOMs in coordinating neural activity. Furthermore, in addition to the monosynaptic projection from vHPC to mPFC already discussed, a direct projection from the dHPC to mPFC has also been reported (Ye et al., 2017). Future studies will be useful in examining whether SOM interneuron mediated feedforward inhibition or feedback inhibition predominates in supporting long-range synchrony between the HPC and mPFC during spatial working memory.

STAR METHODS

CONTACT FOR REAGENT AND RESOURCE SHARING

Further information and requests for resources and reagents should be directed to and will be fulfilled by the Lead Contact, Atheir Abbas (aia2114@cumc.columbia.edu).

EXPERIMENTAL MODEL AND SUBJECT DETAILS

All procedures were conducted in accordance with the US NIH Guide for the Care and Use of Laboratory Animals and approved by the New York State Psychiatric Institute Institutional Animal Care and Use Committee at Columbia University. All experiments were carried out in male PV-Cre or SOM-Cre mice. The PV-Cre mice used in these studies had been generated as described previously(Lovett-Barron et al., 2012) and were obtained as a hybrid C57BL/6–129/SV strain. PV-Cre mice used in experiments were hemizygous offspring of hemizygous hybrid PV-Cre mice that had been backcrossed to C57BL/6J mice (Jackson Labs, stock number 000664) for 1–3 generations. SOM-Cre mice were also a hybrid C57BL/6–129/SV strain obtained from Jackson Labs (stock number 013044). Hemizygous SOM-Cre offspring of SOM-Cre x C57BL/6J breeding pairs were used for experiments. Mice were 8–12 weeks of age at the start of experiments and housed under a 12-hour light-dark cycle in a temperatureand humidity-controlled environment with food and water available *ad libitum* except when food restricted for spatial working memory. Implanted mice were individually housed. During behavioral habituation, training, and testing, mice were food restricted and maintained at 80–85% of their initial weight.

METHOD DETAILS

Surgical Procedures—Mice were anesthetized with 1–3% vaporized isoflurane in oxygen (1L/min) and placed in a stereotaxic apparatus. For immunochemistry and microdrive implantation experiments PV-Cre or SOM-Cre mice were injected with Cre-inducible Archaerhodopsin (AAV5-EF1a-DIO-eArch3.0-EYFP, UNC vector core) or control EYFP virus (AAV5-EF1a-DIO-EYFP, UNC vector core) at two locations within the mPFC bilaterally (+/−0.35 ML, +1.85 AP, 1.3 and 1.7 depth below brain surface; 0.5 μL virus per injection site). For immunochemistry experiments, mice were first anesthetized with a ketamine (100 mg/kg) and xylazine (7 mg/kg) mixture. The animals were then perfused with 4% paraformaldehyde (Thermo Fisher Scientific) 6–8 weeks after viral injection, and the brains were extracted and cryoprotected in 30% sucrose in 1X PBS until they sank. 40 micron sections were taken in a cryostat and stored in 1X PBS at 4°C until they were used for immunochemistry experiments. The following antibodies and dilutions were used: guinea pig polyclonal anti-parvalbumin (1:2500, Synaptic Systems, 195–004), goat polyclonal anti-somatostatin (1:50, Santa Cruz Biotechnology SC-7819), chicken polyclonal anti-GFP (1:500, Abcam, ab13970), Alexa Fluor 488 goat anti-chicken (1:200, Thermo Fisher Scientific, A-11039), Cy3 donkey anti-guinea pig (1:200, Jackson ImmunoResearch, 706–165-148), Cy3 donkey anti-goat (1:200, Jackson ImmunoResearch 705–166-147). For microdrive implantation experiments, animals were habituated, shaped, and trained as described below, taken off food restriction, and then about 4 weeks after initial viral injection, underwent a second surgery to implant the microdrive. Animals were again anesthetized and placed in a stereotaxic apparatus. Craniotomies were made to allow for implantation of a bundle of 14 stereotrodes (13 micron tungsten wire, California Fine Wire) and a 200 micron optical fiber in the left mPFC (−0.35 ML, +1.85 AP, 1.3 below brain surface); a 200 micron optical fiber in the right mPFC; local field potential (LFP) wires (76 micron tungsten wire) in the vHPC (−3.0 ML, −3.15 AP, 3.9 below brain surface), dHPC (−1.25 ML, +1.82 AP, 1.45 below brain surface), and MD (−0.3 ML, −1.22 AP, 2.7 below brain surface); a ground screw over the cerebellum; and a reference screw over the orbitofrontal cortex. Electrodes were connected to a 32 channel omnetics board, and the board and wires were fixed to an advanceable custom microdrive. Electrode placements were confirmed by passing current through an electrode at each site (5 mA, 10 seconds) to generate an electrothermolytic lesion. Mice were anesthetized with ketamine/xylazine prior to generating the lesions and were then perfused. The brains were extracted, cryoprotected, sectioned, mounted, stained, and examined under a microscope to determine lesion placements and characterize YFP and Arch expression in PL/IL.

Optogenetics—532 nm wavelength light (OEM laser) was delivered at 10 mW via 200 μM diameter, 0.22 NA optical fibers. There were four different trial types: laser off, laser on sample (laser was on the entire sample phase - from when the mouse left the start box to when the mouse returned to the start after retrieving the reward), laser on delay (for the entire delay phase, 10 or 60 seconds), and laser on choice (for the entire choice phase -from when the mouse leaves the start box at the end of the delay phase to when it reaches the reward port) trials. Because prolonged Arch inhibition has been shown to induce rebound activity (Madisen et al., 2012), we measured post-inhibition firing. Even after SOM

inhibition during 60 second delay periods, we did not measure rebound firing that was greater than the baseline firing rate prior to the delay period (Figure S2E).

Behavior—1 week after viral injection, mice were placed on a food-restricted diet and received 2–3 g of food daily as needed to maintain their weight at 80–85% of their day pre-restriction weight. The experimenter monitoring the mice during behavior in a custom, automated T-maze was blinded as to whether the mouse received Arch or control YFP virus. Mice underwent two days of habituation in which they were allowed to freely visit all the baited arms (condensed milk diluted 1:3 in deionized water) in the T-maze for 10 min. They subsequently underwent 2 consecutive days of shaping in which mice were forced to alternate runs to each goal arm (20 runs total) to obtain a reward. Then mice were then transitioned to training, in which they underwent 10 trials daily. During training trials, mice are forced randomly during the sample (working memory encoding) phase to one of the goal arms to obtain milk reward. They then return for a ten second delay period (working memory maintenance). After the delay, both goals are accessible during the choice phase (working memory retrieval), but in order to obtain a reward the mouse has to choose the arm not visited during the sample phase. Mice are considered to have reached criterion once they have achieved three consecutive days of 70% or better performance with respect to making correct choices. Mice underwent 40 testing trials daily for 3–5 days at each delay (10s and 60s), with 10 each of laser off, sample laser on, delay laser on, and choice laser on trials, randomly interleaved for trial type and sample arm. Stereotrodes were advanced at least 40 μM after testing in order to record new single units each day.

Neural Recordings—A Digital Lynx system (Neuralynx, Bozeman, MT) was used to amplify, bandpass filter (1–1000 Hz for LFPs and 600–6000 Hz for spikes), and digitize the electrode recordings. LFP sampling rates were 2 kHz and spikes were collected at 32 kHz. Single units were clustered based on the first two principal components (peak and energy) from each channel using Klustakwik (Ken Harris) and visualized in SpikeSorter3D (Neuralynx). Clusters were then visually inspected and included or eliminated based on waveform appearance, inter-spike interval distribution, isolation distance, and L-ratio.

Power, coherence, phase locking analysis, and directionality analysis—To calculate power, after normalizing the raw LFP data to the root mean square of the voltage signal over the whole testing session, the power spectra of the LFPs were calculated with a Chronux MATLAB function that used the multi-taper method. For band-specific coherence, the mean coherence over the range was calculated (theta 412 Hz, beta 12–25 Hz, gamma 30–70 Hz). For phase locking analysis, we started by digitally band-pass filtering the raw LFPs using a zero phase delay filter (K. Harris and G. Buzsaki). The phase was calculated using a Hilbert transform, and then a corresponding phase was assigned to each spike. We limited our analysis to units that fired at least 100 times over the period analyzed. Pairwise Phase Consistency (PPC) was calculated as the mean of the cosine of the absolute angular distances between all unique pairs of spike phases. Delta PPC was calculated by subtracting the PPC calculated during trials in which SOM or PV interneurons were not inhibited from the PPC calculated during trials in which SOM or PV interneurons were inhibited during sample, delay, or choice phases (delta PPC). Negative delta PPC values indicate that PPC

has a decrease in phase locking whereas positive delta PPC values indicate an increase in phase locking after SOM or PV inhibition.

Functional directionality was calculated based on PPC of mPFC spikes assigned corresponding spike phases of vHPC and dHPC theta oscillations. We successively calculated PPC of mPFC spikes to vHPC and dHPC theta signals that were shifted in 2.5 ms steps +/− 100 ms. We compared the mean PPC at negative lags to the mean PPC at positive lags, with negative lag PPC > positive lag PPC signifying HPC-->mPFC directionality.

Single Unit Analysis Including Preferred Arm Firing Analysis, Delay-Elevated Analysis, and Decoding—Significantly light-modulated units were identified by bootstrapping. Laser on and laser off spikes were combined, binned, and randomly shuffled 30,000 times. Units were considered light-responsive if the observed laser off vs laser on firing rate difference was greater than 99% of the firing rate differences from the shuffled data. To distinguish between excitatory projection neurons and inhibitory interneurons, which likely account for most of the inhibited neurons, we attempted to utilize unbiased clustering using two or three waveform parameters as previously reported (Courtin et al., 2014; Kim et al., 2016). We attempted this first with the PV-Arch data. However, we were unable to achieve clear cell separation (Figure S1I, top and bottom panel). We also plotted the waveform parameters of “increaser” (putative pyramidal neurons) and “decreaser” (putative PV interneurons) cells, and we found that first sorting cells by response to light and then plotting waveform parameters also does not result in two distinct clusters on 2 dimensional or 3 dimensional waveform parameter plots (Figure S1J, top and bottom panel). This is consistent with a prior study showing that over 50% of PV interneurons as identified by optical tagging with channelrhodopsin are broadspiking and/or have slow after-hyperpolarizations (Moore and Wehr, 2013). Because of these findings we did not attempt clustering with the SOM-Arch data, and we used response to light (significant increase or decrease in firing rate) as the criteria to separate cells in SOM-Arch and PV-Arch animals for further analysis.

In order to measure the strength and reliability of the neural representation of Tmaze spatial location, we first separated arm-preferring neurons as those with a greater than 20% increase in the mean firing during the period from 5 seconds before to 5 seconds after sample goal arrival, using z-scored firing rates calculated in 100 ms bins - mean firing rate within a bin was z-scored to the mean firing rate across a 5 second period of the ITI; standard deviation was calculated within bins as well. We also used a maximum margin linear classifier to decode goal location from binned population firing rate vectors as previously described (Spellman et al., 2015). Analysis was performed on units with at least one training and one testing trial and with 100 repetitions at each time bin. Spike bin size was 200 ms.

Delay-modulated activity was determined based on a previous report (Bolkan et al., 2017). Briefly, it was delay-elevated cells were identified using z-scored firing rates for each neuron calculated in 1 second bins and z-scored to the ITI and standard deviation across bins. Delay-modulated units were defined as those with a change in the z-scored firing rate that is +/− 2 standard deviations for two or more consecutive bins. To assess the effect of SOM and PV inhibition on delay-modulated activity, we compared the distribution of timing of peak

firing rates across neurons between the different laser conditions using the Kolmogorov-Smirnov test and also sorted delaymodulated units in laser off trials into neurons whose transient peak took place from 110 s, 11–20 s, 21–40s, and 41–60s. We then compared the mean firing rate across trial types (laser off, laser on sample, laser on delay, and laser on choice).

QUANTIFICATION AND STATISTICAL ANALYSIS

Statistical analysis was performed in Graphpad Prism 7 or MATLAB. For behavioral experiments and decoding, two-way repeated measures ANOVA was used to assess, depending on the experiment, the effect of light condition (laser off, sample laser on, delay laser on, or choice laser on) and virus type (Arch-EYFP vs EYFP) or light condition and task phase (sample laser on, choice laser on) and the interaction between the two factors in behavioral experiments. Other analyses that required statistically comparing more than two groups in which there was only one factor (for example, laser condition), one-way ANOVA was performed. For both one- and two-way ANOVA analyses, Bonferroni corrected two-tailed tests were performed to make posthoc paired comparisons. For paired laser off and laser on comparisons we used the non-parametric Wilcoxon matched-pairs signed-rank test Bonferroni corrected for multiple comparisons - for example comparing the average power or coherence within a frequency band or the mean across the entire spectrum. To determine the effect of SOM inhibition during the delay period on delay tiling, we used a Kolmogorov-Smirnov to compare the distributions of timing of peak firing across delay-modulated neurons during the delay period to assess whether they were significantly different. For determining which neurons exhibited a significant change in firing rate in response to light, the alpha level was 0.01; for all other analyses, the alpha level was 0.05. For power spectra and coherence, correction for multiple comparisons was performed for all comparisons within a group of animals (i.e., SOM-Arch, PV-Arch, SOM-YFP, PV-YFP). Error bars represent the standard error of the mean. Shaded error bands represent 95% confidence intervals.

Supplementary Material

Refer to Web version on PubMed Central for supplementary material.

Acknowledgements

We thank members of the Gordon and Kellendonk labs for technical assistance and discussions. This work was supported by grants from the NIMH (R01 MH096274 to J.A.G. and T32 MH018870–29 to A.I.A.); by the Leon Levy Foundation (to A.I.A.); a BBRF/NARSAD Young Investigator Grant (A.I.A.); and by the Irma Hirschl Trust (to C.K.).

Appendix

KEY RESOURCES TABLE

REAGENT or RESOURCE	SOURCE	IDENTIFIER
Antibodies		

REAGENT or RESOURCE	SOURCE	IDENTIFIER
guinea pig polyclonal anti-parvalbumin	Synaptic Systems	cat #: 195-004; RRID:AB_2156476
goat polyclonal anti-somatostatin	Santa Cruz Biotechnology	cat #: SC-7819
chicken polyclonal anti-GFP	Abcam	cat #: ab13970; RRID:AB_300798
Alexa Fluor 488 goat anti-chicken	Thermo Fisher Scientific	cat #: A-11039; RRID:AB_2534096
Cy3 donkey anti-guinea pig	Jackson ImmunoResearch	cat #: 706-165-148; RRID:AB_2340460
Cy3 donkey anti-goat	Jackson ImmunoResearch	cat #: 705-166-147; RRID:AB_2307351
Bacterial and Virus Strains		
AAV5-EF1a-DIO-eArch3.0-EYFP	UNC Vector Core	https://www.med.unc.edu/genetherapy/vectorcore/in-stock-aav-vectors/deisseroth
AAV5-EF1a-DIO-EYFP	UNC Vector Core	https://www.med.unc.edu/genetherapy/vectorcore/in-stock-aav-vectors/deisseroth
Experimental Models: Organisms/Strains		
SOM-Cre	Jackson Laboratories	stock #: 013044; RRID: IMSR_JAX:013044
PV-Cre	a gift from Rene Hen, mice originally generated by Boris Zemelman	N/A
C57BL/6	Jackson Laboratories	stock #: 000664; RRID: IMSR_JAX:000664
Software and Algorithms		
Matlab	Mathworks	https://www.mathworks.com/products/matlab/; RRID:SCR_001622
Graphpad Prism 7.02	GraphPad Software	https://www.graphpad.com/scientific-software/prism/; RRID:SCR_002798

References

Akhlaghpour H, Wiskerke J, Choi JY, Taliaferro JP, Au J, and Witten IB (2016). Dissociated sequential activity and stimulus encoding in the dorsomedial striatum during spatial working memory. Elife 5.

Arts B, Jabben N, Krabbendam L, and van Os J (2008). Meta-analyses of cognitive functioning in euthymic bipolar patients and their first-degree relatives. Psychol Med 38, 771–785. [PubMed: 17922938]

Atallah BV, Bruns W, Carandini M, and Scanziani M (2012). Parvalbuminexpressing interneurons linearly transform cortical responses to visual stimuli. Neuron 73, 159–170. [PubMed: 22243754]

Bolkan SS, Stujenske JM, Parnaudeau S, Spellman TJ, Rauffenbart C, Abbas AI, Harris AZ, Gordon JA, and Kellendonk C (2017). Thalamic projections sustain prefrontal activity during working memory maintenance. Nat Neurosci 20, 987–996. [PubMed: 28481349]

Brekke JS, Hoe M, Long J, and Green MF (2007). How neurocognition and social cognition influence functional change during community-based psychosocial rehabilitation for individuals with schizophrenia. Schizophr Bull 33, 1247–1256. [PubMed: 17255120]

Canetta S, Bolkan S, Padilla-Coreano N, Song LJ, Sahn R, Harrison NL, Gordon JA, Brown A, and Kellendonk C (2016). Maternal immune activation leads to selective functional deficits in offspring parvalbumin interneurons. Mol Psychiatry 21, 956–968. [PubMed: 26830140]

Carlen M, Meletis K, Siegle JH, Cardin JA, Futai K, Vierling-Claassen D, Ruhlmann C, Jones SR, Deisseroth K, Sheng M, et al. (2012). A critical role for NMDA receptors in parvalbumin interneurons for gamma rhythm induction and behavior. Mol Psychiatry 17, 537–548. [PubMed: 21468034]

Chow BY, Han X, Dobry AS, Qian X, Chuong AS, Li M, Henninger MA, Belfort GM, Lin Y, Monahan PE, et al. (2010). High-performance genetically targetable optical neural silencing by light-driven proton pumps. Nature 463, 98–102. [PubMed: 20054397]

Churchwell JC, and Kesner RP (2011). Hippocampal-prefrontal dynamics in spatial working memory: interactions and independent parallel processing. Behav Brain Res 225, 389–395. [PubMed: 21839780]

Courtin J, Chaudun F, Rozeske RR, Karalis N, Gonzalez-Campo C, Wurtz H, Abdi A, Baufreton J, Bienvenu TC, and Herry C (2014). Prefrontal parvalbumin interneurons shape neuronal activity to drive fear expression. Nature 505, 92–96. [PubMed: 24256726]

Fujisawa S, Amarasingham A, Harrison MT, and Buzsaki G (2008). Behaviordependent short-term assembly dynamics in the medial prefrontal cortex. Nat Neurosci 11, 823–833. [PubMed: 18516033]

Fung SJ, Fillman SG, Webster MJ, and Shannon Weickert C (2014). Schizophrenia and bipolar disorder show both common and distinct changes in cortical interneuron markers. Schizophr Res 155, 26–30. [PubMed: 24674775]

Fung SJ, Webster MJ, Sivagnanasundaram S, Duncan C, Elashoff M, and Weickert CS (2010). Expression of interneuron markers in the dorsolateral prefrontal cortex of the developing human and in schizophrenia. Am J Psychiatry 167, 1479–1488. [PubMed: 21041246]

Gandal MJ, Sisti J, Klook K, Ortinski PI, Leitman V, Liang Y, Thieu T, Anderson R, Pierce RC, Jonak G, et al. (2012). GABAB-mediated rescue of altered excitatory-inhibitory balance, gamma synchrony and behavioral deficits following constitutive NMDAR-hypofunction. Transl Psychiatry 2, e142. [PubMed: 22806213]

Gentet LJ, Kremer Y, Taniguchi H, Huang ZJ, Staiger JF, and Petersen CC (2012). Unique functional properties of somatostatin-expressing GABAergic neurons in mouse barrel cortex. Nat Neurosci 15, 607–612. [PubMed: 22366760]

Green MF (2016). Impact of cognitive and social cognitive impairment on functional outcomes in patients with schizophrenia. J Clin Psychiatry 77 Suppl 2, 8–11. [PubMed: 26919052]

Green MF, Kern RS, Braff DL, and Mintz J (2000). Neurocognitive deficits and functional outcome in schizophrenia: are we measuring the “right stuff”? Schizophr Bull 26, 119–136. [PubMed: 10755673]

Guise KG, and Shapiro ML (2017). Medial Prefrontal Cortex Reduces Memory Interference by Modifying Hippocampal Encoding. Neuron 94, 183–192 e188. [PubMed: 28343868]

Hallock HL, Wang A, and Griffin AL (2016). Ventral Midline Thalamus Is Critical for Hippocampal-Prefrontal Synchrony and Spatial Working Memory. J Neurosci 36, 8372–8389. [PubMed: 27511010]

Hashimoto T, Arion D, Unger T, Maldonado-Aviles JG, Morris HM, Volk DW, Mirnics K, and Lewis DA (2008). Alterations in GABA-related transcriptome in the dorsolateral prefrontal cortex of subjects with schizophrenia. Mol Psychiatry 13, 147–161. [PubMed: 17471287]

Hashimoto T, Volk DW, Eggan SM, Mirnics K, Pierri JN, Sun Z, Sampson AR, and Lewis DA (2003). Gene expression deficits in a subclass of GABA neurons in the prefrontal cortex of subjects with schizophrenia. J Neurosci 23, 6315–6326. [PubMed: 12867516]

Horst NK, and Laubach M (2012). Working with memory: evidence for a role for the medial prefrontal cortex in performance monitoring during spatial delayed alternation. J Neurophysiol 108, 3276–3288. [PubMed: 23019007]

Jones MW, and Wilson MA (2005). Theta rhythms coordinate hippocampalprefrontal interactions in a spatial memory task. PLoS Biol 3, e402. [PubMed: 16279838]

Kamigaki T, and Dan Y (2017). Delay activity of specific prefrontal interneuron subtypes modulates memory-guided behavior. Nat Neurosci 20, 854–863. [PubMed: 28436982]

Keefe RS, Silva SG, Perkins DO, and Lieberman JA (1999). The effects of atypical antipsychotic drugs on neurocognitive impairment in schizophrenia: a review and meta-analysis. Schizophr Bull 25, 201–222. [PubMed: 10416727]

Kim D, Jeong H, Lee J, Ghim JW, Her ES, Lee SH, and Jung MW (2016). Distinct Roles of Parvalbumin- and Somatostatin-Expressing Interneurons in Working Memory. Neuron 92, 902–915. [PubMed: 27746132]

Kvitsiani D, Ranade S, Hangya B, Taniguchi H, Huang JZ, and Kepecs A (2013). Distinct behavioural and network correlates of two interneuron types in prefrontal cortex. Nature 498, 363–366. [PubMed: 23708967]

Jelem A, and Klausberger T (2016). Divisions of Identified Parvalbumin-Expressing Basket Cells during Working Memory-Guided Decision Making. Neuron 91, 1390–1401. [PubMed: 27593181]

Lai CL, Lau Z, Lui SS, Lok E, Tam V, Chan Q, Cheng KM, Lam SM, and Cheung EF (2016). Meta-analysis of neuropsychological measures of executive functioning in children and adolescents with high-functioning autism spectrum disorder. Autism Res.

Landro NI, Stiles TC, and Sletvold H (2001). Neuropsychological function in nonpsychotic unipolar major depression. Neuropsychiatry Neuropsychol Behav Neurol 14, 233–240. [PubMed: 11725217]

Lee I, and Kesner RP (2003). Time-dependent relationship between the dorsal hippocampus and the prefrontal cortex in spatial memory. J Neurosci 23, 1517–1523. [PubMed: 12598640]

Lovett-Barron M, Turi GF, Kaifosh P, Lee PH, Bolze F, Sun XH, Nicoud JF, Zemelman BV, Sternson SM, and Losonczy A (2012). Regulation of neuronal input transformations by tunable dendritic inhibition. Nat Neurosci 15, 423–430, S421–423. [PubMed: 22246433]

Madisen L, Mao T, Koch H, Zhuo JM, Berenyi A, Fujisawa S, Hsu YW, Garcia AJ, 3rd, Gu X, Zanella S, et al. (2012). A toolbox of Cre-dependent optogenetic transgenic mice for light-induced activation and silencing. Nat Neurosci 15, 793–802. [PubMed: 22446880]

Martinussen R, H.J., Hogg-Johnson S, Tannock R (2005). A meta-analysis of working memory impairments in children with attention-deficit/hyperactivity disorder. J Am Acad Child Adolesc Psychiatry 44, 377–384. [PubMed: 15782085]

Mattis J, Tye KM, Ferenczi EA, Ramakrishnan C, O'Shea DJ, Prakash R, Gunaydin LA, Hyun M, Fenno LE, Gradinaru V, et al. (2011). Principles for applying optogenetic tools derived from direct comparative analysis of microbial opsins. Nat Methods 9, 159–172. [PubMed: 22179551]

Moore AK, and Wehr M (2013). Parvalbumin-expressing inhibitory interneurons in auditory cortex are well-tuned for frequency. J Neurosci 33, 13713–13723. [PubMed: 23966693]

Murray AJ, Woloszynowska-Fraser MU, Ansel-Bollepalli L, Cole KL, Foggetti A, Crouch B, Riedel G, and Wulff P (2015). Parvalbumin-positive interneurons of the prefrontal cortex support working memory and cognitive flexibility. Sci Rep 5, 16778. [PubMed: 26608841]

O'Neill PK, Gordon JA, and Sigurdsson T (2013). Theta oscillations in the medial prefrontal cortex are modulated by spatial working memory and synchronize with the hippocampus through its ventral subregion. J Neurosci 33, 14211–14224. [PubMed: 23986255]

Parent MA, Wang L, Su J, Netoff T, and Yuan LL (2010). Identification of the hippocampal input to medial prefrontal cortex in vitro. Cereb Cortex 20, 393–403. [PubMed: 19515741]

Park S, and Holzman PS (1992). Schizophrenics show spatial working memory deficits. Arch Gen Psychiatry 49, 975–982. [PubMed: 1449384]

Parnaudeau S, O'Neill PK, Bolkan SS, Ward RD, Abbas AI, Roth BL, Balsam PD, Gordon JA, and Kellendonk C (2013). Inhibition of mediodorsal thalamus disrupts thalamofrontal connectivity and cognition. Neuron 77, 1151–1162. [PubMed: 23522049]

Rajan K, Harvey CD, and Tank DW (2016). Recurrent Network Models of Sequence Generation and Memory. Neuron 90, 128–142. [PubMed: 26971945]

Rigotti M, Barak O, Warden MR, Wang XJ, Daw ND, Miller EK, and Fusi S (2013). The importance of mixed selectivity in complex cognitive tasks. Nature 497, 585–590. [PubMed: 23685452]

Saykin AJ, Gur RC, Gur RE, Mozley PD, Mozley LH, Resnick SM, Kester DB, and Stafiniak P (1991). Neuropsychological function in schizophrenia. Selective impairment in memory and learning. Arch Gen Psychiatry 48, 618–624. [PubMed: 2069492]

Saykin AJ, Shtasel DL, Gur RE, Kester DB, Mozley LH, Stafiniak P, and Gur RC (1994). Neuropsychological deficits in neuroleptic naive patients with first-episode schizophrenia. Arch Gen Psychiatry 51, 124–131. [PubMed: 7905258]

Schmitt LI, Wimmer RD, Nakajima M, Happ M, Mofakham S, and Halassa MM (2017). Thalamic amplification of cortical connectivity sustains attentional control. Nature 545, 219–223. [PubMed: 28467827]

Sigurdsson T, Stark KL, Karayiorgou M, Gogos JA, and Gordon JA (2010). Impaired hippocampal-prefrontal synchrony in a genetic mouse model of schizophrenia. Nature 464, 763–767. [PubMed: 20360742]

Silberberg G, and Markram H (2007). Disynaptic inhibition between neocortical pyramidal cells mediated by Martinotti cells. Neuron 53, 735–746. [PubMed: 17329212]

Spellman T, Rigotti M, Ahmari SE, Fusi S, Gogos JA, and Gordon JA (2015). Hippocampal-prefrontal input supports spatial encoding in working memory. Nature 522, 309–314. [PubMed: 26053122]

Taniguchi H, He M, Wu P, Kim S, Paik R, Sugino K, Kvitsiani D, Fu Y, Lu J, Lin Y, et al. (2011). A resource of Cre driver lines for genetic targeting of GABAergic neurons in cerebral cortex. Neuron 71, 995–1013. [PubMed: 21943598]

Urban-Ciecko J, and Barth AL (2016). Somatostatin-expressing neurons in cortical networks. Nat Rev Neurosci 17, 401–409. [PubMed: 27225074]

Urban KR, Layfield DM, and Griffin AL (2014). Transient inactivation of the medial prefrontal cortex impairs performance on a working memory-dependent conditional discrimination task. Behav Neurosci 128, 639–643. [PubMed: 25314661]

Wall NR, De La Parra M, Sorokin JM, Taniguchi H, Huang ZJ, and Callaway EM (2016). Brain-Wide Maps of Synaptic Input to Cortical Interneurons. J Neurosci 36, 4000–4009. [PubMed: 27053207]

Wang GW, and Cai JX (2006). Disconnection of the hippocampal-prefrontal cortical circuits impairs spatial working memory performance in rats. Behav Brain Res 175, 329–336. [PubMed: 17045348]

Yavorska I, and Wehr M (2016). Somatostatin-Expressing Inhibitory Interneurons in Cortical Circuits. Front Neural Circuits 10, 76. [PubMed: 27746722]

Ye X, Kapeller-Libermann D, Travaglia A, Inda MC, and Alberini CM (2017). Direct dorsal hippocampal-prelimbic cortex connections strengthen fear memories. Nat Neurosci 20, 52–61. [PubMed: 27869801]

Highlights

- mPFC PV and SOM inhibition modulates neuronal activity and synchrony within mPFC
- PV inhibition does not impair spatial working memory
- SOM inhibition during working memory encoding decreases choice accuracy
- SOM inhibition decreases long-range HPC-mPFC synchrony and spatial encoding

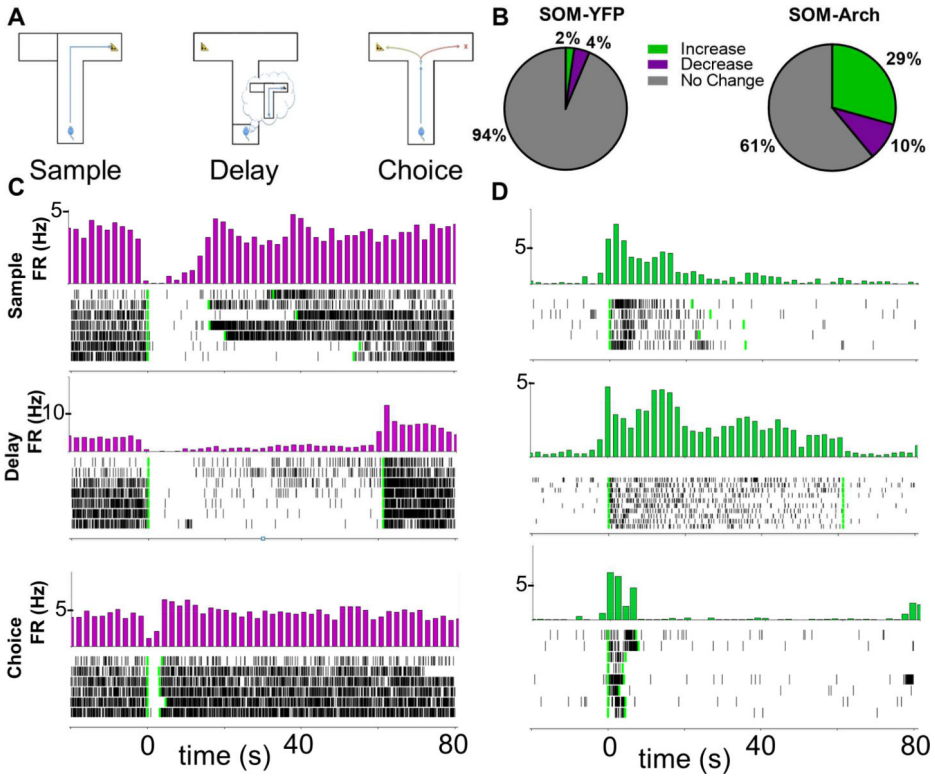

Figure 1: Archaerhodopsin Inhibition of SOM Interneurons Decreases Interneuron Firing and Increases Pyramidal Cell Firing

A.) Schematic for T-maze delayed-non-match-to-sample test. Neural recordings are obtained during this spatial working memory task. B.) Proportions of cells with a significant increase or decrease in firing rate in response to sample phase green light as determined by bootstrapping ($p<0.01$) in SOM-YFP (N =394 cells) and SOM-Arch (N = 382 cells) animals. C.) Time triggered average (green light turns on at time = 0, marked by first vertical green line; green light turns off at second vertical green line) and raster plot of a cell inhibited by Archaerhodopsin during sample, delay, and choice phases. D.) Time triggered average and raster plot of a cell that is disinhibited during SOM interneuron inhibition in sample, delay, and choice phases.

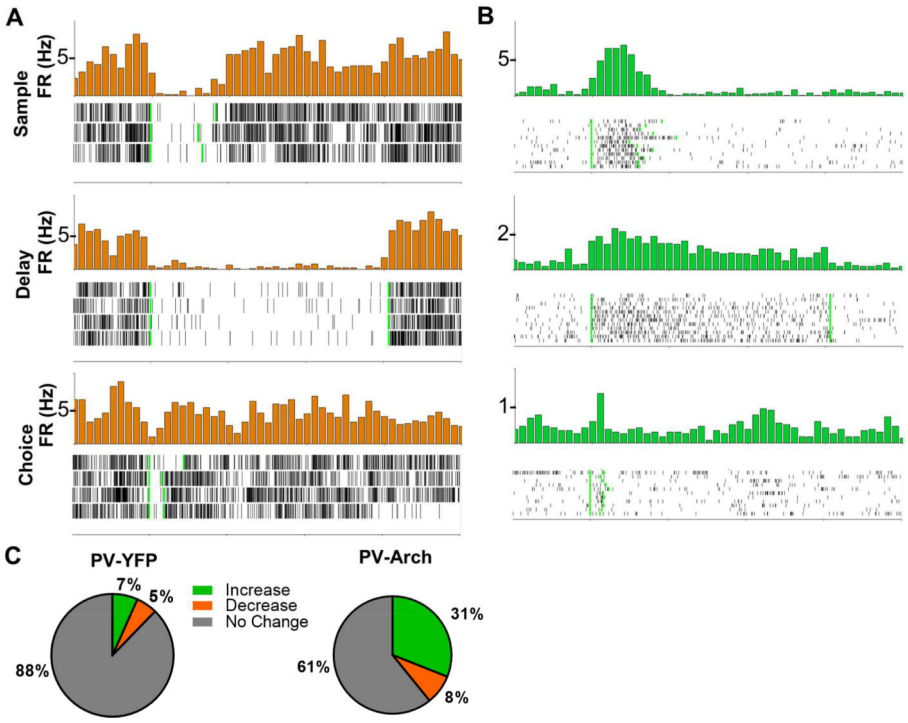

Figure 2: Archaerhodopsin Inhibition of PV Interneurons Decreases Interneuron Firing and Increases Pyramidal Cell Firing

A.) Time triggered average (green light turns on at time = 0, marked by first vertical green line; green light turns off at second vertical green line) and raster plot of a cell inhibited by Archaerhodopsin during the sample, delay, and choice phases. B.) Time triggered average and raster plot of a cell disinhibited during PV interneuron inhibition during the sample, delay, and choice phases. C.) Proportions of cells with a significant increase or decrease in firing rate in response to sample phase green light as determined by bootstrapping in PV-YFP (N = 179 cells) or PV-Arch (N = 244 cells) animals.

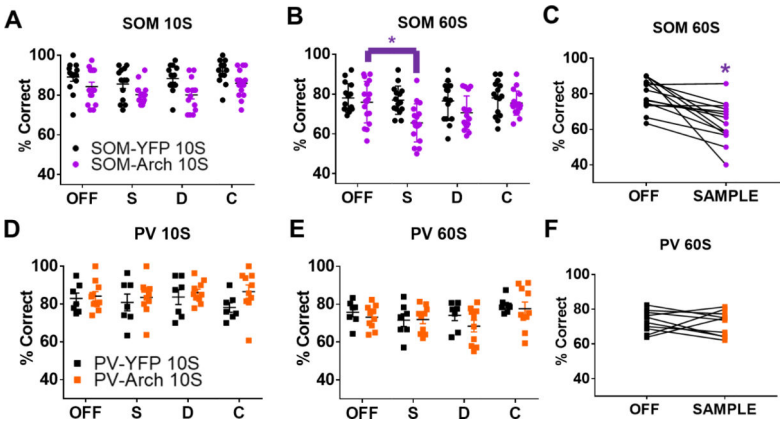

Figure 3: Inhibiting SOM Interneurons During Working Memory Encoding Impairs Performance

Above, "OFF" refers to trials in which the laser was off. "S" or "Sample", "D", and "C" refer to trials in which the laser was on during the sample, delay, or choice phase, respectively. Inhibiting SOM interneurons during the DNMTS spatial working memory task does not significantly impair performance when the delay is A.) 10 seconds, but does significantly impair performance when the delay is B.) and C.) 60 seconds. Inhibiting PV interneurons during sample, delay, or choice phases of the task does not impair spatial working memory performance at D.) 10 second or E.) and F.) 60 second delay. See main text for summary of statistics.

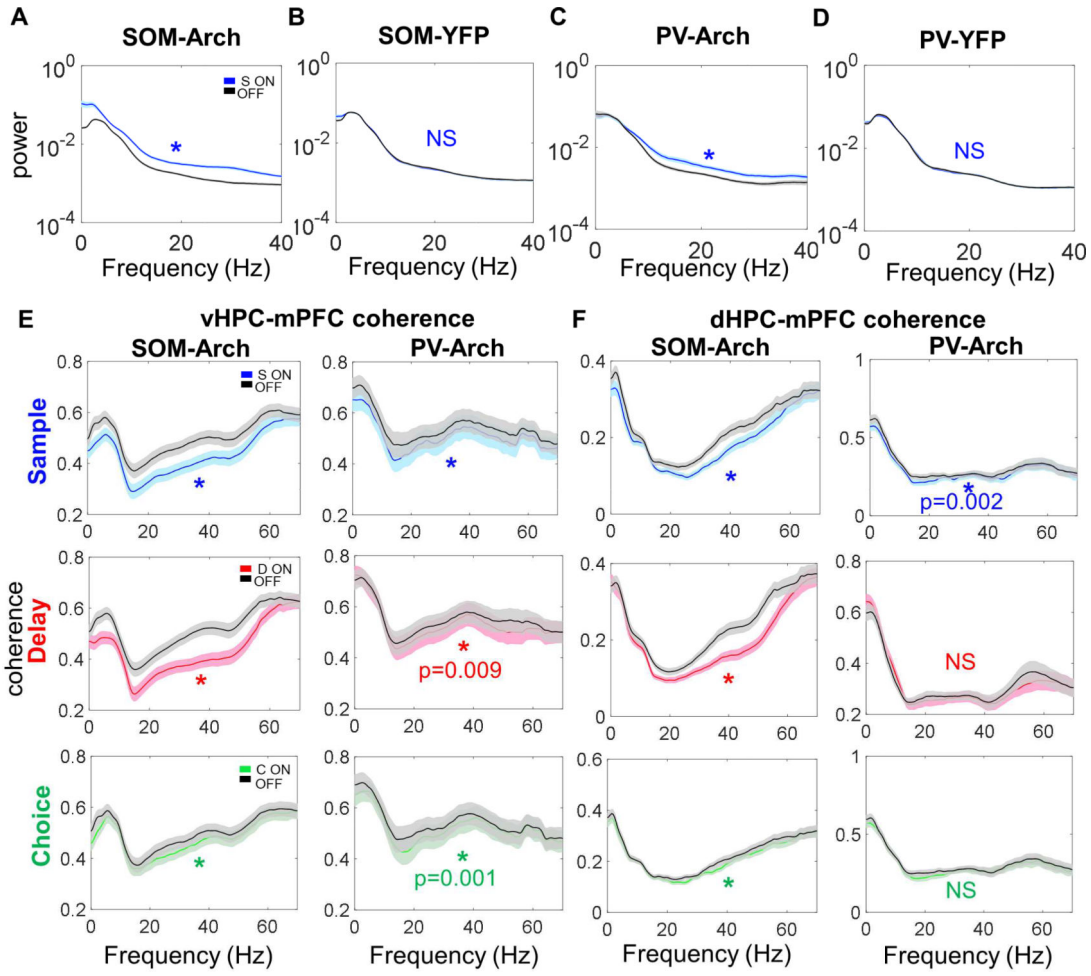

Figure 4: Inhibiting SOM and PV Interneurons Leads to Decreased vHPC-mPFC Coherence and dHPC-mPFC Coherence

A.) Inhibiting SOM interneurons in SOM-Arch mice during the sample phase leads to a broadband increase in power (dark lines in this figure represent the mean, with the lighter shaded band representing the 95% confidence interval; for all comparisons in this figure, significance was determined by two-tailed Wilcoxon matched-pairs signed rank test Bonferroni corrected for multiple comparisons; unless otherwise indicated here and throughout, * indicates $p<0.0001$). B.) Green light during the sample phase in SOMYFP mice does not affect mPFC power. C.) Inhibiting PV interneurons in PV-Arch mice during the sample phase leads to a broadband increase in power. D.) Green light during the sample phase in PV-YFP mice does not affect mPFC power. E.) Left column, Inhibiting SOM interneurons during the sample, delay, and choice phases decreases vHPC-mPFC coherence over a wide range of frequencies. Right column, Inhibiting PV interneurons during sample, delay, and choice phases generally leads to a smaller decrease in vHPC-mPFC coherence than that seen with SOM inhibition. F.) Left column, Inhibiting SOM interneurons during the sample, delay, and choice phases decreases dHPC-mPFC coherence. Right column, Inhibiting PV interneurons during the sample, but not delay or choice phases, leads to a small decrease in dHPC-mPFC coherence.

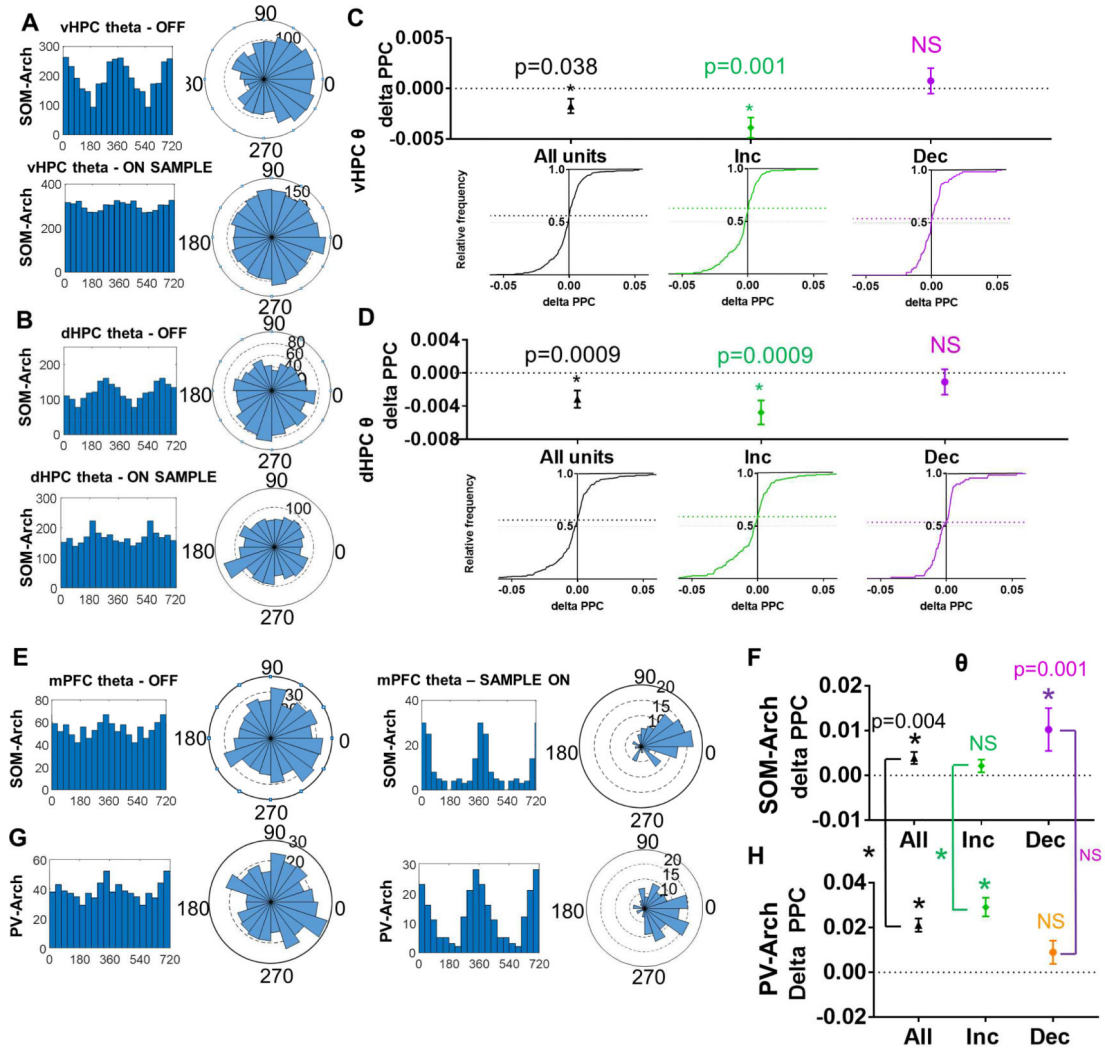

Figure 5: Inhibiting SOM Interneurons During the Sample Phase Leads to Decreased Phase Locking of mPFC Units to vHPC and dHPC Theta and Decreased Phase Locking to Local mPFC Theta

A.) Histogram and rose plots illustrating a decrease in phase locking of mPFC single units to vHPC theta oscillations during SOM-inhibited trials (see bottom row) as compared to non-inhibited trials (see top row). B.) Histogram and rose plots illustrating a decrease in phase locking of mPFC single units to dHPC theta oscillations during SOM-inhibited trials (see bottom row) as compared to non-inhibited trials (see top row). C-D.) Cumulative frequency distribution of delta PPC (Pairwise Phase Consistency; Sample ON PPC – Sample OFF PPC) calculated for all single units (left column, black), units that increase in response to SOM inhibition (middle column, green), and units that decrease in response to SOM inhibition (right column, purple). When calculating phase locking of mPFC units to C.) vHPC theta and D.) dHPC theta, the frequency distribution skews towards negative delta PPC values for all units and increasers, but not for decreasers (data in C-H are represented as mean ± SEM; statistical comparisons in this figure between ON and OFF by Wilcoxon matched-pairs signed rank test Bonferroni corrected for multiple comparisons). E.) Histogram and rose plots illustrating an increase in phase locking of mPFC single units to

mPFC theta oscillations during SOMinhibited trials (see right column) as compared to non-inhibited trials (see left columns). F.) SOM inhibition leads to a significant increase in phase locking of mPFC units to local mPFC theta oscillations as illustrated by delta PPC (PPC SAMPLE ON – PPC SAMPLE OFF) values that are significantly greater than zero. G.) Histogram and rose plots illustrating a decrease in phase locking of mPFC single units to dHPC theta oscillations during PV-inhibited trials (see bottom row) are compared to non-inhibited trials (see top row). H.) PV inhibition also leads to a significant increase in phase locking of mPFC units to local mPFC theta oscillations which is significantly greater than that seen in SOM-Arch mice when comparing all cells and increasers (comparisons signified by the vertical lines between F and H, * $p<0.0001$).

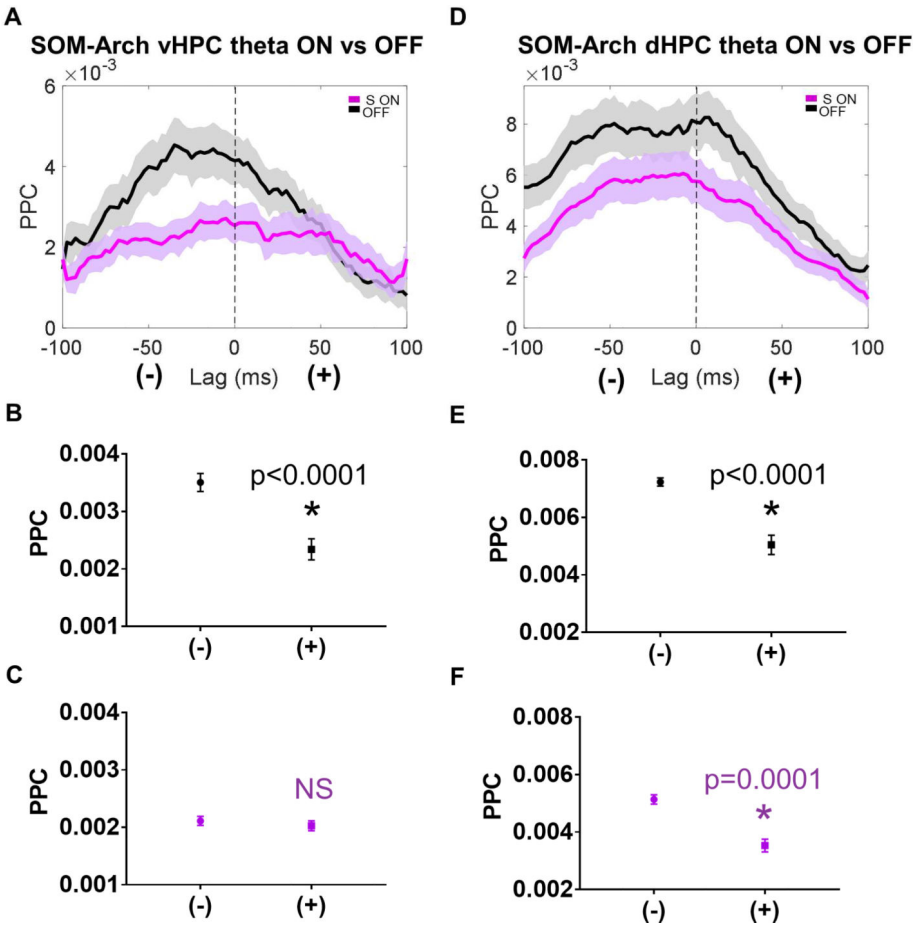

Figure 6: Sample Phase SOM Inhibition impairs vHPC to mPFC Directionality During Long Range Synchronization

A.) mPFC units exhibit higher phase locking to negative lag vHPC theta as compared to positive lag vHPC theta during the sample phase, but this directionality is abolished by SOM inhibition (dark lines in A and D represent the mean, with the lighter shaded band representing the 95% confidence interval). B.) During the sample phase in OFF trials, the mean PPC at negative lags is significantly greater than the mean PPC at positive lags (data in B-C and E-F are represented as mean ± SEM; statistical comparisons between mean PPC at negative vs positive lags is by Wilcoxon matched-pairs signed rank test Bonferroni corrected for multiple comparisons; * indicates $p<0.0001$). C.) During the sample phase in SOM-inhibited trials, there is no significant difference between the mean PPC to vHPC theta at negative vs positive lags. D.) mPFC units exhibit higher phase locking to negative lag dHPC theta as compared to positive lag dHPC theta during the sample phase, both during OFF trials and SOM inhibited trials. E.) and F.) During the sample phase in OFF and SOM inhibited trials, the mean PPC to dHPC theta at negative lags is significantly greater than the mean PPC to dHPC theta at positive lags.

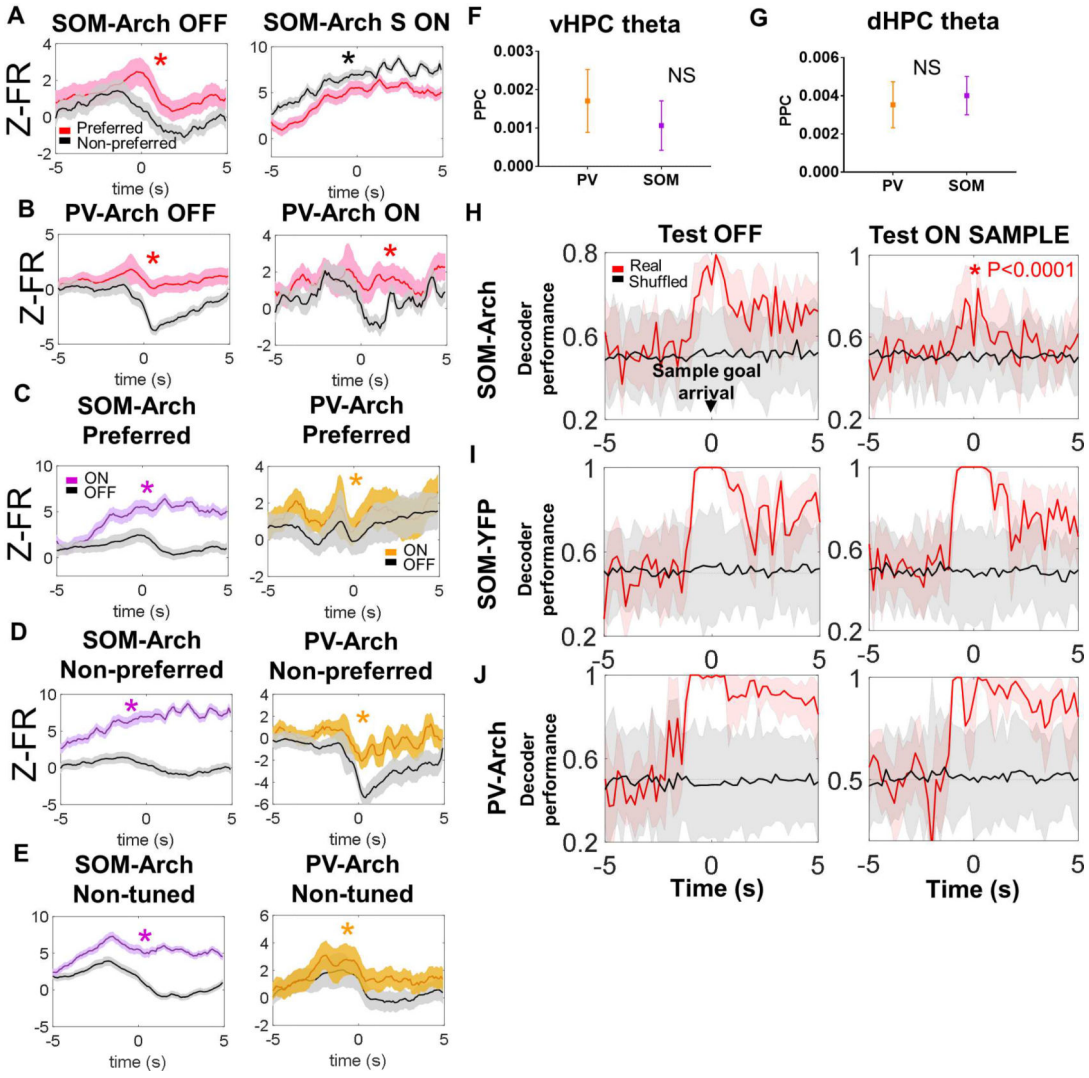

Figure 7: Inhibition SOM but not PV Interneurons Impairs Spatial Encoding in the mPFC

A.) Z-scored firing rate is higher in the preferred arm of spatially tuned neurons during the sample phase around the time of sample goal arrival during laser off trials (left panel; (dark lines in A-E represent the mean, with the lighter shaded band representing the 95% confidence interval) but not during SOM inhibition (right panel; for this panel and others in this figure, asterisks indicate statistical comparisons that are significant by Wilcoxon matched-pairs signed rank test). B.) Z-scored firing rate is higher in the preferred arm of spatially tuned neurons during the sample phase around the time of sample goal arrival during laser off trials (left panel); this spatial tuning is not significantly affected by PV inhibition (right panel). C.-E) Firing rate is significantly increased during laser on (i.e., during SOM or PV inhibition) trials in the preferred and non-preferred arms of spatially tuned cells and in non-spatially tuned cells; this effect appears more robust during SOM inhibition as compared to PV inhibition. F.) and G.) There is no significant difference in phase locking of SOMs and PVs to vHPC theta or dHPC theta oscillations (data in F-G are represented as mean ± SEM). H.) Sample goal identity can be decoded from the mPFC population in SOM-Arch mice when the decoder is trained and tested on laser off trials (left

panel; in H- J, solid lines – mean decoder accuracy, shaded areas – 95% confidence intervals), but not as well when the decoder is trained in laser off trials and tested in sample on trials (right panel, asterisk in graph indicates significance by two-way ANOVA followed by Bonferroni-corrected posthoc testing with p-value shown next to asterisk). I.) Sample goal identity can be decoded from the mPFC population in SOM-YFP mice when the decoder is trained and tested on laser off trials (left panel) and when the decoder is trained in laser off trials and tested in sample on trials (right panel). J.) Sample goal identity can also be decoded from the mPFC population in PV-Arch mice when the decoder is trained and tested in laser off trials (left panel) and when the decoder is trained in laser off trials and tested in sample on trials (right panel).

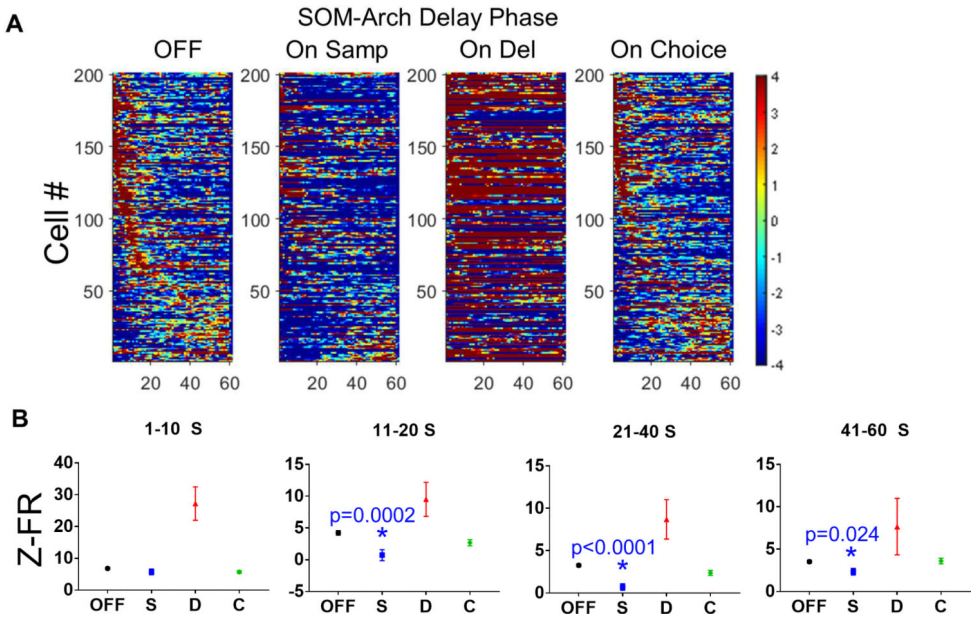

Figure 8: Inhibiting SOMs During the Sample Phase Disrupts Subsequent Delay-Elevated mPFC Activity

A.) Normalized firing rates for delay-elevated mPFC neurons during the delay phase for light OFF trials and On Sample, On Delay, and On Choice trials. Inhibiting SOMs during the sample phase (On Sample trials) appears to disrupt delay-elevated activity. It is difficult to visualize the transient elevations in firing rate when SOMs are inhibited during the delay period (On Delay) due to a large increase in the baseline firing rate for many of the neurons. Delay-elevated mPFC firing during On Choice trials, prior to SOM inhibition, appears to be preserved. B.) SOM inhibition during the sample phase significantly decreases firing rates in delay-elevated neurons during much of the delay period (data in B are represented as mean ± SEM; for cells whose peaks occur during 1–10 S, 11–20 S, and 21–40 S periods; statistical significance was determined by oneway ANOVA with Bonferroni-corrected post-hoc testing; asterisks indicate significance with p-value listed on graph).